



Central London  
HONO budget  
analysis

J. D. Lee et al.

This discussion paper is/has been under review for the journal Atmospheric Chemistry and Physics (ACP). Please refer to the corresponding final paper in ACP if available.

# Detailed budget analysis of HONO in central London reveals a missing daytime source

J. D. Lee<sup>1,2</sup>, L. K. Whalley<sup>3,4</sup>, D. E. Heard<sup>3,4</sup>, D. Stone<sup>4</sup>, R. E. Dunmore<sup>2</sup>,  
J. F. Hamilton<sup>2</sup>, D. E. Young<sup>5,a</sup>, J. D. Allan<sup>5,6</sup>, S. Laufs<sup>7</sup>, and J. Kleffmann<sup>7</sup>

<sup>1</sup>National Centre for Atmospheric Science, WACL Building, University of York, York, UK

<sup>2</sup>Department of Chemistry, University of York, York, UK

<sup>3</sup>National Centre for Atmospheric Science, University of Leeds, Leeds, UK

<sup>4</sup>School of Chemistry, University of Leeds, Leeds, UK

<sup>5</sup>School of Earth, Atmospheric and Environmental Sciences, University of Manchester, Oxford Road, Manchester, M13 9PL, UK

<sup>6</sup>National Centre for Atmospheric Science, University of Manchester, Oxford Road, Manchester, M13 9PL, UK

<sup>7</sup>Physikalische und Theoretische Chemie/FB C, Bergische Universität Wuppertal (BUW), Gaußstr. 20, 42119 Wuppertal, Germany

<sup>a</sup>now at: Department of Environmental Toxicology, University of California, Davis, CA 95616, USA

Title Page

Abstract

Introduction

Conclusions

References

Tables

Figures



Back

Close

Full Screen / Esc

Printer-friendly Version

Interactive Discussion



Received: 18 June 2015 – Accepted: 23 July 2015 – Published: 18 August 2015

Correspondence to: J. D. Lee (james.lee@york.ac.uk)

Published by Copernicus Publications on behalf of the European Geosciences Union.

**ACPD**

15, 22097–22139, 2015

**Central London  
HONO budget  
analysis**

J. D. Lee et al.

Title Page

Abstract

Introduction

Conclusions

References

Tables

Figures



Back

Close

Full Screen / Esc

Printer-friendly Version

Interactive Discussion



## Abstract

Measurements of HONO were carried out at an urban background site near central London as part of the *Clean air for London* (ClearfLo) project in summer 2012. Data was collected from 22 July–18 August 2014, with peak values of up to 1.8 ppbV at night and non-zero values of between 0.2 and 0.6 ppbV seen during the day. A wide range of other gas phase, aerosol, radiation and meteorological measurements were made concurrently at the same site, allowing a detailed analysis of the chemistry to be carried out. The peak HONO/NO<sub>x</sub> ratio of 0.04 is seen at ~ 02:00 UTC, with the presence of a second, daytime peak in HONO/NO<sub>x</sub> of similar magnitude to the night-time peak suggesting a significant secondary daytime HONO source. A photostationary state calculation of HONO involving formation from the reaction of OH and NO and loss from photolysis, reaction with OH and dry deposition shows a significant underestimation during the day, with calculated values being close to zero, compared to the measurement average of 0.4 ppbV at midday. The addition of further HONO sources, including postulated formation from the reaction of HO<sub>2</sub> with NO<sub>2</sub> and photolysis of HNO<sub>3</sub>, increases the daytime modelled HONO to 0.1 ppbV, still leaving a significant extra daytime source. The missing HONO is plotted against a series of parameters including NO<sub>2</sub> and OH reactivity, with little correlation seen. Much better correlation is observed with the product of these species with  $j(\text{NO}_2)$ , in particular NO<sub>2</sub> and the product of NO<sub>2</sub> with OH reactivity. This suggests the missing HONO source is in some way related to NO<sub>2</sub> and also requires sunlight. The effect of the missing HONO to OH radical production is also investigated and it is shown that the model needs to be constrained to measured HONO in order to accurately reproduce the OH radical measurements.

## 1 Introduction

The hydroxyl radical (OH) is the main daytime oxidant in the troposphere, playing a key role in the chemical transformations of trace species (Levy II, 1971). A major source

ACPD

15, 22097–22139, 2015

### Central London HONO budget analysis

J. D. Lee et al.

Title Page

Abstract

Introduction

Conclusions

References

Tables

Figures



Back

Close

Full Screen / Esc

Printer-friendly Version

Interactive Discussion





**Central London  
HONO budget  
analysis**

J. D. Lee et al.

Title Page

Abstract

Introduction

Conclusions

References

Tables

Figures



Back

Close

Full Screen / Esc

Printer-friendly Version

Interactive Discussion



aerosols or the ground itself. Major ground surfaces were recently confirmed by direct flux measurements of HONO (Ren et al., 2011; Zhou et al., 2011; Zhang et al., 2012). It is postulated that such processes involve the conversion of  $\text{NO}_2$  or  $\text{HNO}_3$  to HONO on ground surfaces and are enhanced by sunlight, thus providing a daytime only source of HONO (Zhou et al., 2003; George et al., 2005). In addition, bacterial production of nitrite in soil surfaces were also proposed as additional HONO source (Su et al., 2011; Oswald et al., 2013). It has also been shown that HONO is emitted directly from petrol and diesel vehicle exhausts (Kurtenbach et al., 2001; Li et al., 2008), although at most sites (with the exception of those adjacent to major roads or in tunnels), this is a relatively small contributor to HONO due to its relatively short atmospheric lifetime in the daytime (10–20 min). Recent reviews of the possible daytime HONO sources are given in Kleffmann (2007) and Michoud et al. (2014).

Almost all previous field studies still show a significant missing daytime HONO source, thus showing the requirement for more studies. In this work we report what are, to our knowledge, the first measurements of HONO made in London, UK, one of the largest cities in Europe. The measurements were made as part of the summer intensive operation period of the *Clean Air for London* (ClearLo) project and, as a result, were made concurrently with a wide range of other atmospheric gas and aerosol phase species (including OH,  $\text{HO}_2$ , NO,  $\text{NO}_2$  and photolysis rates). This has enabled us to undertake a detailed modelling study of HONO using the Master Chemical Mechanism (MCMv3.2), with subsequent investigation of potential missing sources. The model was also used to assess the radical forming potential of the missing HONO, which can ultimately lead to increased production of secondary pollutants such as ozone ( $\text{O}_3$ ) and secondary organic aerosol (SOA).

## 2 Experimental

The Clean air for London (ClearLo) project had the aim of providing an integrated measurement and modelling program in order to help better understand the atmospheric



**Central London  
HONO budget  
analysis**

J. D. Lee et al.

Title Page

Abstract

Introduction

Conclusions

References

Tables

Figures

◀

▶

◀

▶

Back

Close

Full Screen / Esc

Printer-friendly Version

Interactive Discussion



glass inlet was only 2 cm minimizing sampling artefacts. The LOPAP has two stripping coils connected in series to correct interferences. In the first coil (channel 1), HONO is trapped quantitatively together with a small amount of the interfering substances. Assuming that these interfering species are trapped in a similar amount in the second coil (channel 2), the difference between the signals of the two channels provides an interference-free HONO signal. Zero measurements were performed every 7 h. Calibrations of the spectrometer using a known concentration of the derivatized azo dye were carried out 3 times during the campaign. The instrument was previously successfully validated against the spectroscopic DOAS technique under urban conditions and in a smog chamber (Kleffmann et al., 2006). During the campaign a detection limit of 1 pptV (for a time resolution of 5 min), a precision of 1 % and an accuracy of 10 % were obtained.

### 2.3 Radical measurements

OH, HO<sub>2</sub> and RO<sub>2</sub> radical concentrations were measured using the FAGE (fluorescence assay by gas expansion) technique (Heard and Pilling, 2003). In the case of HO<sub>2</sub> and RO<sub>2</sub>, the radicals were first titrated with NO to OH before FAGE detection. The current mode of operation will be described in detail elsewhere (Whalley et al., 2015). The HO<sub>2</sub> observations used as a constraint in the modelling studies reported in Sect. 3.3 were made using a low flow of NO (7.5 sccm), which laboratory tests have shown minimised interferences from alkene and aromatic-derived RO<sub>2</sub> species (Whalley et al., 2013). Under this regime, the interference from RO<sub>2</sub> radicals present is estimated to contribute < 3 % to the HO<sub>2</sub> concentration. The limit of detection (LOD) at a signal to noise ratio of one for one data acquisition cycle was  $\sim 4.5 \times 10^5$  molecule cm<sup>-3</sup> for OH and  $\sim 2.1 \times 10^6$  molecule cm<sup>-3</sup> for HO<sub>2</sub>. The measurements were recorded with 1 s time-resolution, and the accuracy of the measurements was  $\sim 15$  %.

## 2.4 Other supporting measurements

The NO and NO<sub>2</sub> data used in this work were taken using an Air Quality Design Inc. custom built high sensitivity chemiluminescence analyser with LED based blue light NO<sub>2</sub> converter. The instrument consists of two channels measuring NO by reaction with excess O<sub>3</sub> to form excited state NO<sub>2</sub> followed by the detection of the resultant chemiluminescence (Drummond et al., 1985; Lee et al., 2009). The air flow in one of the channels first passes through a photolytic converter where light at 395 nm from an array of LEDs photolyses NO<sub>2</sub> to NO. The 395 nm wavelength has a specific affinity for NO<sub>2</sub> photolytic conversion to NO, giving high analyte selectivity within the channel and there is a low probability of other species (such as HONO) being photolysed (Pollack et al., 2010). This makes this measurement a significant improvement over the high temperature catalytic NO<sub>2</sub> conversion used for the long term measurement at the North Kensington site (Steinbacher et al., 2007; Villena et al., 2012). Calibration of the instrument was carried out every 2 days using 5 ppm NO in nitrogen (BOC – certified to NPL scale) – diluted to ~ 20 ppb using high purity zero air (BOC BTCA 178). The NO<sub>2</sub> conversion efficiency was calibrated using gas phase titration of the NO standard by O<sub>3</sub>. NO<sub>y</sub> data were taken using a TEI 42i TL NO analyser with Molybdenum converter. VOC measurements were obtained using two gas chromatography (GC) instruments. The volatile fraction of VOCs (C<sub>2</sub>–C<sub>7</sub> hydrocarbons, with a small selection of OVOCs) was measured using a dual channel (DC)-GC-FID (Hopkins et al., 2003), while a comprehensive two dimensional GC (GC × GC-FID) measured the less volatile fraction (C<sub>6</sub>–C<sub>13</sub>, with a large group of OVOCs) (Lidster et al., 2014). Measurements of HCHO were made using an Aerolaser 4021 analyser (Salmon et al., 2008). Briefly gaseous formaldehyde is scrubbed into the liquid phase via a stripping coil containing dilute sulphuric acid. This is followed by reaction with Hantzsch reagent, a dilute solution made with acetyl acetone, acetic acid, and ammonium acetate. Aqueous phase formaldehyde reacts with this reagent via the “Hantzsch Reaction” to produce 3,5-diacetyl-1,4-dihydrolutidine (DDL). Once excited by an appropriate wavelength (400 nm

### Central London HONO budget analysis

J. D. Lee et al.

Title Page

Abstract

Introduction

Conclusions

References

Tables

Figures



Back

Close

Full Screen / Esc

Printer-friendly Version

Interactive Discussion



in this case), DLL fluoresces thus allowing quantitative assay by monitoring the emitted light. Non refractory nitrate and ammonium aerosol measurements were taken using a compact time-of-flight aerosol mass spectrometer (cToF-AMS – Aerodyne Inc.), which gave data with a time resolution of 5 min (Young et al., 2015).

Actinic fluxes of solar radiation were measured using a spectral radiometer, which consisted of an Ocean Optics high resolution spectrometer (QE65000), couple via fibre optic to a  $2\pi$  quartz collection dome. These measurements were then used to calculate the photolysis frequencies of a number of > 50 trace gases, including  $\text{NO}_2$ , HONO and  $\text{O}_3$  ( $j(\text{O}^1\text{D})$ ) (Kraus and Hofzumahaus, 1998; Edwards and Monks, 2003). Wind speed and direction, temperature and relative humidity were measured using a Davis Vantage Vue met station. Mixing heights estimation was based on the vertical profiles of the hourly vertical velocity variance (Barlow et al., 2011). The vertical velocity variance was measured with a Doppler Lidar (Halo-Photonics scanning Doppler lidar) located at the North Kensington site with a gate resolution of 18 m; the un-sampled portion of the vertical velocity variance is calculated with the spectral correction technique described in (Barlow et al., 2015). The mixing height is defined as the height up to which the vertical velocity variance is higher than  $0.1 \text{ m}^2 \text{ s}^{-2}$ . This threshold value was perturbed by 20 %, (i.e. between  $0.08$  and  $0.121 \text{ m}^2 \text{ s}^{-2}$ ) and the median of the estimated values was taken as the hourly mixing height.

## 3 Results

### 3.1 Overview of data

Data were collected from 22 July–18 August 2012 and time series of local wind speed, wind direction,  $\text{NO}$ ,  $\text{NO}_2$ ,  $\text{O}_3$ , HONO and the photolysis rate of HONO ( $j(\text{HONO})$ ) are shown in Fig. 1. The majority of the measurement period was characterised by south westerly winds, with the wind speed showing a diurnal cycle of less than  $1 \text{ m s}^{-1}$  at night (the minimum measurable by the anemometer) to  $4\text{--}6 \text{ m s}^{-1}$  in late afternoon.

Title Page

Abstract

Introduction

Conclusions

References

Tables

Figures



Back

Close

Full Screen / Esc

Printer-friendly Version

Interactive Discussion



**Central London  
HONO budget  
analysis**

J. D. Lee et al.

Title Page

Abstract

Introduction

Conclusions

References

Tables

Figures



Back

Close

Full Screen / Esc

Printer-friendly Version

Interactive Discussion



These periods show NO and NO<sub>2</sub> with peaks of 15 and 10 ppbV respectively, typically at ~ 07:30 UTC, the peak of the morning rush hour. O<sub>3</sub> shows a diurnal cycle with a typical maximum of 40–45 ppbV at ~ 16:00 UTC and minima of < 20 ppbV at night. The exception to this are two periods from 24–27 July and 8–10 August, during which the site was subjected to generally easterly flow, with lower wind speed. Due to central London being to the East of the site, these periods are characterised by higher levels of NO<sub>x</sub> (up to 60 ppbV of NO and 50 ppbV of NO<sub>2</sub>), which has its source mainly from traffic exhaust. O<sub>3</sub> is also higher during these periods, due to a combination of the higher primary pollution levels (NO<sub>x</sub> and VOCs) and low wind speeds causing a build-up of this secondary pollutant during the 3–4 day period. Peak daytime levels of O<sub>3</sub> of 60–100 ppbV are observed during these more polluted periods. HONO concentrations show peak values at night throughout the campaign (up to 1.8 ppbV during the easterly periods and up to 0.7 ppbV during the rest of the campaign), with non-zero values seen during the day (0.3–0.6 ppbV).

This behaviour is better visualised using the average diurnal cycle, which is shown for HONO and NO<sub>x</sub> in Fig. 2a and  $j(\text{HONO})$  and the HONO/NO<sub>x</sub> ratio in Fig. 2b. As well as the total campaign average, diurnal cycles are shown for the easterly and westerly time periods described above. NO<sub>x</sub> follows an expected profile, with a peak of 29 ppbV on average during the morning rush hour at ~ 05:30 UTC (06:30 LT), followed by a decrease during the day, due largely to increasing boundary layer depth and hence dilution. After ~ 16:00 UTC, the NO<sub>x</sub> levels begin to rise from a minimum of 8.5 ppbV, due to a combination of increased emissions during the evening rush hour and the reduction of the boundary layer depth into the night. Concentrations reach ~ 18 ppbV by midnight and remain reasonably constant throughout the rest of the night. Diurnal averages in the easterly and westerly conditions follow the same pattern as for the total data series, with significantly higher NO<sub>x</sub> during the easterly period. During the morning peak, NO<sub>x</sub> is a factor of 3 higher during easterly flow compared to westerly and 15–20 % higher during the daytime. HONO appears to follow a similar diurnal profile to NO<sub>x</sub>, which is not unexpected since the main known HONO sources involve nitro-

**Central London  
HONO budget  
analysis**

J. D. Lee et al.

Title Page

Abstract

Introduction

Conclusions

References

Tables

Figures



Back

Close

Full Screen / Esc

Printer-friendly Version

Interactive Discussion



gen oxides. However, the morning peak of HONO is around 1 h earlier compared to  $\text{NO}_x$  (at around 04:30) due to the onset of HONO photolysis at sunrise. HONO concentrations are also higher under easterly flow conditions compared to westerly, with the early morning peak being a factor of around 2 higher and the daytime average around 25 % higher. The behaviour of HONO is perhaps better described by looking at the HONO/ $\text{NO}_x$  ratio and the average diurnal cycle of HONO/ $\text{NO}_x$  and  $j(\text{HONO})$  is shown in Fig. 2b. The peak HONO/ $\text{NO}_x$  of 0.04 is seen at  $\sim 02:00$  UTC, due to the lack of photolysis (the major loss route for HONO), direct HONO emissions and heterogeneous HONO formation at the surface during the night, into a relatively shallow boundary layer. After this (and before sunrise), the ratio begins to decrease due to the onset of fresh  $\text{NO}_x$  emissions and continues to decrease during the morning due to the increase of HONO photolysis. The presence of a second, daytime peak in HONO/ $\text{NO}_x$  of similar magnitude to the nighttime peak suggests a significant secondary and probably photo-enhanced, HONO source.

The HONO levels measured in London are within the range of data published from other urban sites, although there is a wide range of concentrations reported in the literature. Michoud et al. (2014) reported daytime levels of 0.11 ppbV (averaged for 3 h around local solar noon) at a site near Paris, France, which is lower than our value of 0.44 ppbV. However the site was 14 km from the centre of Paris (upwind), significantly further away from the major emission sources than the London site. As a result,  $\text{NO}_x$  was lower in Paris, with a daytime campaign average of 5.3 ppbV compared to our value of 13.9 ppbV, giving a daytime HONO/ $\text{NO}_x$  ratio of 0.020 compared to our value of 0.031, although this maybe partially explained by the lower  $j(\text{HONO})$  values in London compared to Paris. The fact that the London site is closer to emission sources will most likely also influence this, as direct emission of HONO from traffic exhaust is potentially a significant proportion of HONO in large cities (Kurtenbach et al., 2001). Some other studies in large cities have reported even larger daytime HONO concentrations, e.g. Santiago, Chile (1.5 ppbV) (Elshorbany et al., 2009), Guangzhou, China (2.0 ppbV) (Qin et al., 2009) and Xinken, China (0.80 ppbV) (Su et al., 2008a, b), however all of

these were at sites with much larger  $\text{NO}_x$  loading, with the resultant  $\text{HONO}/\text{NO}_x$  ratio being similar to the measurements in London. The range of ambient HONO values reported in the literature suggest that the specific conditions at a particular site are key to the HONO levels and hence a modelling study is required for gaining a full understanding of its behaviour.

### 3.2 HONO photostationary state approach

In order to initially assess HONO concentrations and in particular the impact of any potential extra sources during this campaign, a photostationary state (PSS) calculation has been carried out. In this approach, the sources and sinks of the species in question are assumed to balance each other and is thus only suitable for species with a short lifetime, such as free radicals. However, it has been widely used to study the daytime HONO budget, despite its lifetime being in the range of 10–20 min during the day (Alicke et al., 2002; Wong et al., 2012), resulting in significant uncertainties, especially for measurements close to emission sources (Lee et al., 2013). However, the measurement site in this study is described as an urban background site and thus is relatively free from the influence of major roads or point sources. Calculation of the photochemical lifetime using the  $\text{NO}_x/\text{NO}_y$  ratio (using the technique described in Cappa et al., 2012) shows a lifetime since emission of 40–50 min, significantly greater than the lifetime of HONO (typically 10–20 min at noon). Thus, we consider the PSS approach still as a useful tool to quantify HONO sources during daytime.

During daytime, HONO is expected to be in photostationary state due to its formation by the reaction between OH and NO, and its sinks by rapid photolysis (to reform OH and NO), its reaction with OH and its dry deposition. Combining these terms, the concentration  $[\text{HONO}]_{\text{PSS}}$  can be calculated using the following Eq. (1):

$$\text{HONO}_{\text{PSS}} = \frac{k_{\text{OH}+\text{NO}}[\text{OH}][\text{NO}]}{k_{\text{OH}+\text{HONO}}[\text{OH}] + j(\text{HONO}) + \frac{v_{\text{HONO}}}{h}} \quad (1)$$

## Central London HONO budget analysis

J. D. Lee et al.

Title Page

Abstract

Introduction

Conclusions

References

Tables

Figures



Back

Close

Full Screen / Esc

Printer-friendly Version

Interactive Discussion





**Central London  
HONO budget  
analysis**

J. D. Lee et al.

Title Page

Abstract

Introduction

Conclusions

References

Tables

Figures



Back

Close

Full Screen / Esc

Printer-friendly Version

Interactive Discussion



model was run with a sub-set of the MCM and treated the degradation of simultaneously measured trace VOCs, CH<sub>4</sub> and CO following oxidation by OH, O<sub>3</sub> and NO<sub>3</sub> and included ~ 15 000 reactions and ~ 3800 species. The model was constrained to measurements of NO, NO<sub>2</sub>, O<sub>3</sub>, CO, CH<sub>4</sub>, 62 individual VOC species measured by GC-FID and also 2-D-GC, PAN, HCHO, HNO<sub>3</sub>, HO<sub>2</sub>, water vapour, temperature and pressure. The model was constrained with the measured photolysis rates (including  $j(\text{O}^1\text{D})$ ,  $j(\text{NO}_2)$ ,  $j(\text{HONO})$ ,  $j(\text{HCHO})$ ,  $j(\text{CH}_3\text{COCH}_3)$  and  $j(\text{CH}_3\text{CHO})$ ) made using the spectral radiometer. A constant H<sub>2</sub> concentration of 500 ppbV was assumed (Forster et al., 2012). The model inputs were updated every 15 min. For species measured more frequently, data was averaged to 15 min intervals, whilst those measured at a lower time resolution were interpolated. The loss of all non-constrained, model generated, species (apart from HONO) by deposition or mixing was represented as a first order loss rate equivalent to 1 cm s<sup>-1</sup> in a 300 m boundary layer depth.

The model was run for the entirety of the campaign in overlapping 7 day segments. To allow all the unmeasured, model generated intermediate species time to reach steady state concentrations, the model was initialised with inputs from the first measurement day (22 July) for 5 days before comparison to measurements were made. Comparison of these 5 spin up days demonstrated that the concentration of model generated species rapidly converged and there was less than a 1 % difference in (for example) modelled OH or HONO concentration by the second spin up day. As a result of this, the model segments were run so as to overlap for 2 days only to reduce the computing time. The model was run unconstrained to HONO (for the results presented in this paper) for comparison with measured HONO concentration.

A number of HONO sources in addition to the gas phase source from the reaction of hydroxyl radicals with NO have been included in the model. These include:

1. A daytime source from the photolysis of ortho nitro phenols which were not measured during the campaign but have been estimated to be present at an upper limit constant concentration of 1 ppbV and which photolyse at a rate of  $\sim 3 \times 10^{-5} \text{ s}^{-1}$  at midday (Bejan et al., 2006).

**Central London  
HONO budget  
analysis**

J. D. Lee et al.

Title Page

Abstract

Introduction

Conclusions

References

Tables

Figures

◀

▶

◀

▶

Back

Close

Full Screen / Esc

Printer-friendly Version

Interactive Discussion



2. Heterogeneous conversion of  $\text{NO}_2$  to HONO on ground has been parameterised and included in the model taking a ground surface conversion efficiency of 0.03 (Stutz et al., 2002) and  $\text{NO}_2$  deposition velocity of  $1 \text{ cm s}^{-1}$  (Joyce et al., 2014) and the measured boundary layer depth. However, it has to be stressed, that the present calculation strongly underestimates the contribution of heterogeneous HONO formation on ground surfaces, especially during night-time at the measurement height, caused by the assumption of an instantaneous mixing in the whole BL, see Eq. (1). In contrast strong HONO gradients have been observed in night-time atmospheres (e.g. Kleffmann et al., 2003; Wong et al., 2011; VandenBoer et al., 2013) confirming the ground as the main source of HONO during nighttime. Since the measurements of the present study were performed also close to the ground surface the contribution of heterogeneous HONO formation is underestimated in the model. For the more accurate description of the night-time HONO formation, which was not the main topic of this study, models should be used which consider vertical transport.

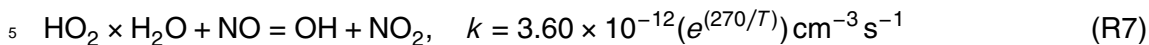
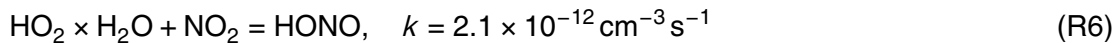
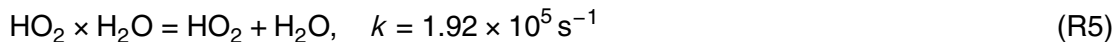
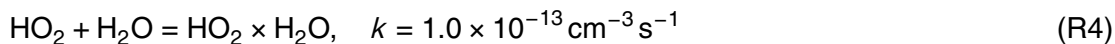
3. Heterogeneous conversion of  $\text{NO}_2$  to HONO on aerosol surfaces was also considered assuming an uptake coefficient of  $10^{-6}$  (Kleffmann et al., 1999; Arens et al., 2001; Monge et al., 2010).

4. Photolysis of  $\text{HNO}_3$  on surfaces has been reported to produce HONO (Zhou et al., 2003, 2011). We have estimated the concentration of  $\text{HNO}_3$  deposited to the ground surface from the gas-phase  $\text{HNO}_3$  concentration that was measured during ClearLo and a deposition velocity of  $\text{HNO}_3$  of  $2 \text{ cm s}^{-1}$  (Zhou et al., 2011). To assess the maximum impact of this potential HONO source, a photolysis rate of surface  $\text{HNO}_3$  which is two orders of magnitude faster than  $j(\text{HNO}_3)$  in the gas phase has been taken (Zhou et al., 2011) for which in addition a 100% HONO yield was assumed.

We did not include photosensitized heterogeneous conversion of  $\text{NO}_2$  on organic substrates like humic acids (George et al., 2005; Stemmler et al., 2006, 2007) into



environment (Reactions R6 and R7):



A direct emission source of HONO was also added to the model, using a ratio of HONO:NO<sub>x</sub> of 0.008 reported previously from tailpipe emission studies of NO<sub>x</sub> and HONO in tunnels (Kurtenbach et al., 2001) and the measured NO<sub>x</sub> concentrations, along with a value of 60% NO<sub>x</sub> estimated to come from traffic emissions in London (take from the UK National Atmospheric Emissions Inventory; Bush et al., 2006). It is likely that the value we use is an upper limit of the direct emission contribution to HONO during daytime, due to the short atmospheric lifetime of HONO (10–20 min) compared to NO<sub>x</sub>.

The full time series of the modelled HONO using the MCM, along with the measured values for the entire measurement campaign are shown in Fig. 4. Due to the difficulties of predicting nighttime chemistry with a photochemical model (such as the MCM), we only consider here the daytime (06:00–20:00). The time series show that predicted daytime HONO using the full model is higher than from the simple PSS calculation, however, it can be seen that the predicted daytime HONO is still significantly lower than the measurement on all days. The average daytime diurnal cycle of the measured and modelled HONO, along with the contribution of the different sources in the model is shown in Fig. 5. From just after sunrise (06:00), the contribution to HONO of the reaction between OH and NO decreases quickly due to the increasing *j*(HONO) throughout the morning. During this time, the HONO sources from direct emissions and the HO<sub>2</sub> × H<sub>2</sub>O + NO<sub>2</sub> reaction are roughly similar in magnitude to the OH+ NO reaction). There are small contributions during the day and from heterogeneous conversion of NO<sub>2</sub> (on both aerosol and ground surfaces) and the photolysis of ortho-nitro-phenol. However, as explained above most probably the HO<sub>2</sub> × H<sub>2</sub>O + NO<sub>2</sub> reaction is overes-

Central London  
HONO budget  
analysis

J. D. Lee et al.

Title Page

Abstract

Introduction

Conclusions

References

Tables

Figures



Back

Close

Full Screen / Esc

Printer-friendly Version

Interactive Discussion



5  
10  
15  
20  
25

estimated here, while the heterogeneous conversion of  $\text{NO}_2$  on ground surfaces is underestimated by the simplified box model approach. Examining the total HONO predicted by the model compared to the measurement shows a significant underestimation of the modelled HONO compared to the measurement. They do both follow a similar diurnal cycle, with a decrease in HONO until around 16:00, followed by an increase into the evening, however the modelled HONO is up to a factor of around 3 lower than the measurement throughout the day. Subtracting the modelled from the measured HONO gives us a quantity that can be described as “missing” HONO, and average diurnal daytime profile of this is plotted in Fig. 6. The amount of missing HONO begins to increase at 06:30 and reaches a maximum at 08:00 of  $\sim 0.35$  ppbV. It then starts to decrease throughout the afternoon and into the evening. Further analysis can be carried out by examining the diurnal profiles in the easterly and westerly flow conditions described earlier. Both conditions show broadly the same diurnal profile, however the daytime peak in missing HONO is significantly greater in the more polluted easterly flow (up to 0.6 ppbV). This suggests that any missing source of HONO is related in some way to the pollution loading, most likely the amount of  $\text{NO}_2$ . This will be discussed further in later sections.

It is clear from this data, that neither a photostationary state calculation nor a more complete photochemical model containing currently known and postulated sources of HONO (that are relevant for this environment) except the photosensitized conversion of  $\text{NO}_2$  on organic ground surfaces (which cannot easily be including in a zero dimensional box model) can reproduce the daytime levels measured in London during this study. This is potentially significant, as HONO can be a large source of free radicals in such an urban environment, and any missing source in models can lead to an underestimation of the oxidising capacity of the atmosphere, and hence its ability to produce  $\text{O}_3$ . Therefore it is worth considering where the “missing” HONO may come from and the importance of any extra source to the atmospheric oxidation capacity.

**Central London  
HONO budget  
analysis**

J. D. Lee et al.

Title Page

Abstract

Introduction

Conclusions

References

Tables

Figures



Back

Close

Full Screen / Esc

Printer-friendly Version

Interactive Discussion





missing HONO, there appears to be a reasonable correlation with the product of  $\text{NO}_2$  and  $j(\text{NO}_2)$ , hence pointing towards a photolytic source.

To further investigate any potential correlation, the full data series of the missing HONO source and different input data are normalised to 1 and correlated against each other. The normalised missing HONO source data are then correlated with the normalised products of all possible combinations of the input data. The datasets are then filtered to determine if inclusion of an extra dataset has led to a genuine increase in the correlation coefficient. For inclusion in the filtered output, the correlation coefficient for the product must be greater than the correlation coefficient for each of the individual components in the product. Additionally, inclusion of an additional dataset in a product must lead to an increase in the correlation coefficient for the new product when compared to the correlation coefficient without that new dataset. Datasets included are:  $j(\text{NO}_2)$ , water vapour, NO,  $\text{NO}_2$ , temperature, adsorbed  $\text{HNO}_3$ , ( $\text{HNO}_{3\text{ads.}}$ ), OH,  $\text{HO}_2$ ,  $\text{RO}_2$ , OH reactivity ( $k(\text{OH})$ ), nitrate aerosol ( $\text{NO}_3^-_{\text{aero.}}$ ), ammonium aerosol ( $\text{NH}_4^+_{\text{aero.}}$ ) and aerosol surface area (SA). The correlation plots are shown in the Supplement (Fig. S1), with the correlation coefficients of the different combinations presented in Table 1. The data shows that several product combinations are significantly higher than those of the individual components, and seem to favour the products of  $j(\text{NO}_2) \times \text{NO}_2$  ( $r^2 = 0.66$ ) and  $j(\text{NO}_2) \times k(\text{OH})$  ( $r^2 = 0.75$ ). A plot of the missing HONO source against the combined product ( $\text{NO}_2 \times k(\text{OH}) \times j(\text{NO}_2)$ ) gives an  $r^2$  of 0.79. In order to investigate the day-to-day variation in the potential HONO source, correlation plots were made of the daytime average (06:00–18:00) missing HONO source against  $\text{NO}_2$  and the product of  $j(\text{NO}_2)$  with  $\text{NO}_2$ ,  $k(\text{OH})$  and  $\text{NO}_2 \times k(\text{OH})$  (Fig. 8). These show that there is some correlation for all species, with the products of the species with  $j(\text{NO}_2)$  ( $r^2 = 0.72$ , 0.73 and 0.77 for  $\text{NO}_2$ ,  $k(\text{OH})$  and  $\text{NO}_2 \times k(\text{OH})$  respectively) being significantly higher than with  $\text{NO}_2$  alone ( $r^2 = 0.52$ ). We therefore suggest that the process or processes responsible for the unknown source of HONO in this particular study are connected with light,  $\text{NO}_2$  and organic matter (represented by  $k(\text{OH})$ ), as described in Stemmler et al. (2006, 2007). Other processes are potentially at work, as shown by the

## Central London HONO budget analysis

J. D. Lee et al.

Title Page

Abstract

Introduction

Conclusions

References

Tables

Figures



Back

Close

Full Screen / Esc

Printer-friendly Version

Interactive Discussion



weaker correlation with  $\text{HNO}_3_{\text{ads}}$  and  $\text{NO}_3^-_{\text{aero}}$ , but these are likely of less importance here. It is, however, clear that at the present urban background site close to central London a significant missing source of HONO is active when compared to the output of a box model containing most known sources.

### 4.3 HONO contribution to atmospheric oxidation

HONO is known to be an important initiation source of OH radicals (Ren et al., 2003, 2006; Dusanter et al., 2009; Elshorbany et al., 2009; Hofzumahaus et al., 2009; Villena et al., 2011; Michoud et al., 2012, 2014), so any extra source that is not well understood or defined in models could have a potentially important impact on atmospheric oxidation capacity and hence  $\text{O}_3$  and secondary organic aerosol (SOA) production. The model described above was used to produce a rate of production analysis (ROPA) for OH radicals during the measurements campaign, with a view to assessing the importance of HONO and in particular the missing HONO source. For this analysis, the ROPA output was plotted for all OH radical sources and the diurnal average for these is shown in Fig. 9. Initially ignoring the missing HONO source, it can be seen that in the early morning shortly after sunrise, HONO is a significant OH source (30–40% of the total, second only to the propagation source of  $\text{NO} + \text{HO}_2$ ). This is due to the build-up of HONO concentrations overnight, followed by its rapid photolysis after sunrise. Then, approaching solar noon, whilst the absolute production rate from HONO photolysis remains relatively constant, the dominant OH source becomes the  $\text{HO}_2 + \text{NO}$  reaction. At solar noon, HONO unconstrained in the model accounts for around 40% of the total OH radical sources and 57% of the  $\text{HO}_x$  initiation sources. During the late afternoon and evening approaching sunset, OH from HONO photolysis again becomes comparable to  $\text{HO}_2 + \text{NO}$ . The photolysis of  $\text{O}_3$  is only a minor component of the total OH radical sources throughout the day, peaking at around 10% in early afternoon. The same holds for the ozonolysis of alkenes which is caused, at least in part, by the low levels of measured alkenes. With the model constrained to the measured HONO, it was possible to add on the effect of the missing HONO source to OH radical production rate

to the diurnal profile. It can clearly be seen that the OH production rate is significantly increased during the daytime when constraining the model to measured HONO, with the most important time being just before solar noon. Here, the OH production rate increases from  $1.9 \times 10^7$  molecule  $\text{cm}^{-3} \text{s}^{-1}$  to  $2.9 \times 10^7$  molecule  $\text{cm}^{-3} \text{s}^{-1}$ , an increase of 65%. This result shows the crucial importance of the missing HONO in the model to HO<sub>x</sub> radical production, which is directly relevant to atmospheric oxidation capacity and O<sub>3</sub> formation.

This importance is also shown when the model is used to calculate OH concentrations, as shown in Fig. 10. If the model is run with PSS calculated HONO, there is a significant under prediction of OH levels (~ 60% during daytime). When the known or postulated HONO sources are included in the model, the predicted OH is increased by a factor of around 1.8. However predicted OH is still 30% lower at noon compared to the measurement, suggesting a missing OH source. It is only when the model is constrained to measured HONO the agreement between measured and modelled OH becomes excellent (< 5% discrepancy at midday) and within the experimental error of the measurements (~ 15%). This clearly demonstrates the need for models to include accurate HONO measurements for further investigation on the missing HONO source to be carried out so that HONO is better characterised by the model.

## 5 Summary and conclusions

In this study a month long time series of HONO levels at an urban background site in London was measured, with average mixing ratios showing a peak in the early morning of ~ 0.6 ppbV and a minimum during early afternoon of ~ 0.18 ppbV. Analysis of the HONO/NO<sub>x</sub> ratio showed a significant secondary peak during daytime, suggesting additional sources of HONO other than the reaction between NO and OH. The presence of a large range of other atmospheric gas and aerosol measurements (including OH and HO<sub>2</sub> radicals), allowed a detailed study of known and postulated production routes of HONO to be undertaken, using both a simple PSS analysis and a box model based

## Central London HONO budget analysis

J. D. Lee et al.

Title Page

Abstract

Introduction

Conclusions

References

Tables

Figures



Back

Close

Full Screen / Esc

Printer-friendly Version

Interactive Discussion



on the MCMv3.2. The calculated HONO shows a significant daytime underestimation of  $\sim 0.2$  ppbV on average, even when recently suggested sources such as the reaction of HO<sub>2</sub> with NO<sub>2</sub> to produce HONO and a direct source from traffic are included, again suggesting a significant missing HONO source. Correlation plots of the missing HONO production rate against various other species measured at the site show a reasonable correlation with the product of  $j(\text{NO}_2)$  with NO<sub>2</sub> and  $k(\text{OH})$ , suggesting that the proposed photosensitized heterogeneous conversion of NO<sub>2</sub> on organic substrates discovered in laboratory studies is a source of HONO under these urban conditions.

The effect of the missing source of HONO to the oxidising capacity of the urban background atmosphere has been investigated using radical rate of production analyses. These show that OH radical production during the day increases by over 100% if measured HONO is used in the model as compared to allowing the model to run unconstrained to HONO. In addition, modelled OH only agreed to the measurements when HONO was constrained to the measurements in the model. This is a significant result and demonstrates the potential importance of a full understanding of the HONO production processes in an urban area such as London in, for example, air quality prediction models.

The results presented here provide further evidence that unknown sources of HONO are present in the urban environment, and they are probably a function of NO<sub>x</sub> and sunlight. It is not possible to conclude exactly the origin of the source from this work, hence further field measurements and, probably more crucially, laboratory studies are needed to investigate these important processes further.

**The Supplement related to this article is available online at  
doi:10.5194/acpd-15-22097-2015-supplement.**

*Acknowledgements.* The authors would like to thank the staff and governors of The Sion Manning RC School, North Kensington, London for hosting the field campaign. Thanks also go to Brian Bandy from the University of East Anglia for HCHO and Janet Barlow and Christoforos

Halios from the University of Reading for boundary layer height data. The work was funded through the UK Natural Environment Research Council (NERC) ClearLo project (grant number NE/H003223/1).

## References

- 5 Acker, K., Möller, D., Wieprecht, W., Meixner, F. X., Bohn, B., Gilge, S., Plass-Dülmer, C., and Berresheim, H.: Strong daytime production of OH from HNO<sub>2</sub> at a rural mountain site, *Geophys. Res. Lett.*, 33, L02809, doi:10.1029/2005gl024643, 2006.
- Alicke, B., Platt, U., and Stutz, J.: Impact of nitrous acid photolysis on the total hydroxyl radical budget during the limitation of oxidant production/pianura padana produzione di ozono study in Milan, *J. Geophys. Res.*, 107, 8196, doi:10.1029/2000jd000075, 2002.
- 10 Arens, F., Gutzwiller, L., Baltensperger, U., Gäggeler, H. W., and Ammann, M.: Heterogeneous reaction of NO<sub>2</sub> on diesel soot particles, *Environ. Sci. Technol.*, 35, 2191–2199, 2001.
- Atkinson, R., Baulch, D. L., Cox, R. A., Crowley, J. N., Hampson, R. F., Hynes, R. G., Jenkin, M. E., Rossi, M. J., and Troe, J.: Evaluated kinetic and photochemical data for atmospheric chemistry: Volume I - gas phase reactions of O<sub>x</sub>, HO<sub>x</sub>, NO<sub>x</sub> and SO<sub>x</sub> species, *Atmos. Chem. Phys.*, 4, 1461–1738, doi:10.5194/acp-4-1461-2004, 2004.
- 15 Barlow, J. F., Dunbar, T. M., Nemitz, E. G., Wood, C. R., Gallagher, M. W., Davies, F., O'Connor, E., and Harrison, R. M.: Boundary layer dynamics over London, UK, as observed using Doppler lidar during REPARTEE-II, *Atmos. Chem. Phys.*, 11, 2111–2125, doi:10.5194/acp-11-2111-2011, 2011.
- Barlow, J. F., Halios, C. H., Lane, S. E., and Wood, C. R.: Observations of urban boundary layer structure during a strong urban heat island event, *Environ. Fluid Mech.*, 15, 373–398, doi:10.1007/s10652-014-9335-6, 2015.
- Bejan, I., Abd El Aal, Y., Barnes, I., Benter, T., Bohn, B., Wiesen, P., and Kleffmann, J.: The photolysis of ortho-nitrophenols: a new gas phase source of HONO, *Phys. Chem. Chem. Phys.*, 8, 2028–2035, doi:10.1039/b516590c, 2006.
- 25 Bigi, A. and Harrison, R. M.: Analysis of the air pollution climate at a central urban background site, *Atmos. Environ.*, 44, 2004–2012, doi:10.1016/j.atmosenv.2010.02.028, 2010.
- Bohnenstengel, S. I., Belcher, S. E., Aiken, A., Allan, J. D., Allen, G., Bacak, A., Bannan, T. J., Barlow, J. F., Beddows, D. C. S., Bloss, W. J., Booth, A. M., Chemel, C., Coceal, O., Di
- 30

## Central London HONO budget analysis

J. D. Lee et al.

Title Page

Abstract

Introduction

Conclusions

References

Tables

Figures



Back

Close

Full Screen / Esc

Printer-friendly Version

Interactive Discussion



## Central London HONO budget analysis

J. D. Lee et al.

Title Page

Abstract

Introduction

Conclusions

References

Tables

Figures



Back

Close

Full Screen / Esc

Printer-friendly Version

Interactive Discussion



Marco, C. F., Dubey, M. K., Faloon, K. H., Fleming, Z. L., Furger, M., Gietl, J. K., Graves, R. R., Green, D. C., Grimmond, C. S. B., Halios, C. H., Hamilton, J. F., Harrison, R. M., Heal, M. R., Heard, D. E., Helfter, C., Herndon, S. C., Holmes, R. E., Hopkins, J. R., Jones, A. M., Kelly, F. J., Kotthaus, S., Langford, B., Lee, J. D., Leigh, R. J., Lewis, A. C., Lidster, R. T., Lopez-Hilfiker, F. D., McQuaid, J. B., Mohr, C., Monks, P. S., Nemitz, E., Ng, N. L., Percival, C. J., Prévôt, A. S. H., Ricketts, H. M. A., Sokhi, R., Stone, D., Thornton, J. A., Tremper, A. H., Valach, A. C., Visser, S., Whalley, L. K., Williams, L. R., Xu, L., Young, D. E., and Zotter, P.: Meteorology, air quality, and health in London: the ClearLo project, *B. Am. Meteorol. Soc.*, 96, 779–804, doi:10.1175/BAMS-D-12-00245.1, 2015.

Bush, T. J., Tsigatakis, I., King, K., and Passant, N. R.: NAEI UK Emission Mapping Methodology 2006, AEATY/ENV/R/2696, available at: [http://uk-air.defra.gov.uk/assets/documents/reports/cat07/0812151643\\_NAEIMappingMethodReport2006.pdf](http://uk-air.defra.gov.uk/assets/documents/reports/cat07/0812151643_NAEIMappingMethodReport2006.pdf) (last access: 14 August 2015), 2006.

Cappa, C. D., Onasch, T. B., Massoli, P., Worsnop, D. R., Bates, T. S., Cross, E. S., Davidovits, P., Hakala, J., Hayden, K. L., Jobson, B. T., Kolesar, K. R., Lack, D. A., Lerner, B. M., Li, S.-M., Mellon, D., Nuaaman, I., Olfert, J. S., Petäjä, T., Quinn, P. K., Song, C., Subramanian, R., Williams, E. J., and Zaveri, R. A.: Radiative absorption enhancements due to the mixing state of atmospheric black carbon, *Science*, 337, 1078–1081, doi:10.1126/science.1223447, 2012.

Creasey, D. J., Heard, D. E., and Lee, J. D.: Absorption cross-section measurements of water vapour and oxygen at 185 nm, Implications for the calibration of field instruments to measure OH, HO<sub>2</sub> and RO<sub>2</sub> radicals, *Geophys. Res. Lett.*, 27, 1651–1654, doi:10.1029/1999gl011014, 2000.

Dentener, F., Williams, J., and Metzger, S.: Aqueous phase reaction of HNO<sub>4</sub>: the impact on tropospheric chemistry, *J. Atmos. Chem.*, 41, 109–134, doi:10.1023/a:1014233910126, 2002.

Dransfield, T. J., Donahue, N. M., and Anderson, J. G.: High-pressure flow reactor product study of the reactions of HO<sub>x</sub> + NO<sub>2</sub>: the role of vibrationally excited intermediates†, *J. Phys. Chem. A*, 105, 1507–1514, doi:10.1021/jp002391+, 2001.

Drummond, J. W., Volz, A., and Ehhalt, D. H.: An optimized chemiluminescence detector for tropospheric NO measurements, *J. Atmos. Chem.*, 2, 287–306, doi:10.1007/bf00051078, 1985.

Dusanter, S., Vimal, D., Stevens, P. S., Volkamer, R., Molina, L. T., Baker, A., Meinardi, S., Blake, D., Sheehy, P., Merten, A., Zhang, R., Zheng, J., Fortner, E. C., Junkermann, W.,

**Central London  
HONO budget  
analysis**

J. D. Lee et al.

Title Page

Abstract

Introduction

Conclusions

References

Tables

Figures



Back

Close

Full Screen / Esc

Printer-friendly Version

Interactive Discussion



Dubey, M., Rahn, T., Eichinger, B., Lewandowski, P., Prueger, J., and Holder, H.: Measurements of OH and HO<sub>2</sub> concentrations during the MCMA-2006 field campaign – Part 2: Model comparison and radical budget, *Atmos. Chem. Phys.*, 9, 6655–6675, doi:10.5194/acp-9-6655-2009, 2009.

5 Edwards, G. D. and Monks, P. S.: Performance of a single-monochromator diode array spectroradiometer for the determination of actinic flux and atmospheric photolysis frequencies, *J. Geophys. Res.*, 108, 8546–8558, 2003.

Elshorbany, Y. F., Kurtenbach, R., Wiesen, P., Lissi, E., Rubio, M., Villena, G., Gramsch, E., Rickard, A. R., Pilling, M. J., and Kleffmann, J.: Oxidation capacity of the city air of Santiago, Chile, *Atmos. Chem. Phys.*, 9, 2257–2273, doi:10.5194/acp-9-2257-2009, 2009.

10 Forster, G. L., Sturges, W. T., Fleming, Z. L., Bandy, B. J., and Emeis, S.: A year of H<sub>2</sub> measurements at Weybourne Atmospheric Observatory, UK, 2012, *Tellus B*, 64, 17771, doi:10.3402/tellusb.v64i0.17771, 2012.

George, C., Strekowski, R. S., Kleffmann, J., Stemmler, K., and Ammann, M.: Photoenhanced uptake of gaseous NO<sub>2</sub> on solid organic compounds: a photochemical source of HONO?, *Faraday Discuss.*, 130, 195–210, doi:10.1039/b417888m, 2005.

Harrison, R. M. and Kitto, A.-M. N.: Evidence for a surface source of atmospheric nitrous acid, *Atmos. Environ.*, 28, 1089–1094, 1994.

15 Heland, J., Kleffmann, J., Kurtenbach, R., and Wiesen, P.: A new instrument to measure gaseous nitrous acid (HONO) in the atmosphere, *Environ. Sci. Technol.*, 35, 3207–3212, doi:10.1021/es000303t, 2001.

Hofzumahaus, A.: Oral presentation during the conference: Atmospheric Chemical Mechanisms “Simple Models – Real World Complexities” December, University of California, Davis, California, USA, 10–12, 2014.

25 Hofzumahaus, A., Rohrer, F., Lu, K. D., Bohn, B., Brauers, T., Chang, C. C., Fuchs, H., Holland, F., Kita, K., Kondo, Y., Li, X., Lou, S., Shao, M., Zeng, L., Wahner, A., and Zhang, Y.: Amplified trace gas removal in the troposphere, *Science*, 324, 1702–1704, 2009.

Hopkins, J. R., Lewis, A. C., and Read, K. A.: A two-column method for long-term monitoring of non-methane hydrocarbons (NMHCs) and oxygenated volatile organic compounds (o-VOCs), *J. Environ. Monitor.*, 5, 8–13, 2003.

30 Jenkin, M. E., Wyche, K. P., Evans, C. J., Carr, T., Monks, P. S., Alfarra, M. R., Barley, M. H., McFiggans, G. B., Young, J. C., and Rickard, A. R.: Development and chamber evaluation

**Central London  
HONO budget  
analysis**

J. D. Lee et al.

Title Page

Abstract

Introduction

Conclusions

References

Tables

Figures



Back

Close

Full Screen / Esc

Printer-friendly Version

Interactive Discussion



of the MCM v3.2 degradation scheme for  $\beta$ -caryophyllene, *Atmos. Chem. Phys.*, 12, 5275–5308, doi:10.5194/acp-12-5275-2012, 2012.

Joyce, P. L., von Glasow, R., and Simpson, W. R.: The fate of  $\text{NO}_x$  emissions due to nocturnal oxidation at high latitudes: 1-D simulations and sensitivity experiments, *Atmos. Chem. Phys.*, 14, 7601–7616, doi:10.5194/acp-14-7601-2014, 2014.

Kleffmann, J.: Daytime sources of nitrous acid (HONO) in the atmospheric boundary layer, *Chem. Phys. Chem.*, 8, 1137–1144, doi:10.1002/cphc.200700016, 2007.

Kleffmann, J., Becker, K. H., Lackhoff, M., and Wiesen, P.: Heterogeneous conversion of  $\text{NO}_2$  on carbonaceous surfaces, *P., Phys. Chem. Chem. Phys.*, 1, 5443–5450, 1999.

Kleffmann, J., Kurtenbach, R., Lörzer, J., Wiesen, P., Kalthoff, N., Vogel, B., and Vogel, H.: Measured and simulated vertical profiles of nitrous acid, Part I: Field measurements, *Atmos. Environ.*, 37, 2949–2955, 2003.

Kleffmann, J., Gavriloaiei, T., Hofzumahaus, A., Holland, F., Koppmann, R., Rupp, L., Schlosser, E., Siese, M., and Wahner, A.: Daytime formation of nitrous acid: a major source of OH radicals in a forest, *Geophys. Res. Lett.*, 32, L05818, doi:10.1029/2005gl022524, 2005.

Kleffmann, J., Lörzer, J. C., Wiesen, P., Kern, C., Trick, S., Volkamer, R., Rodenas, M., and Wirtz, K.: Intercomparison of the DOAS and LOPAP techniques for the detection of nitrous acid (HONO), *Atmos. Environ.*, 40, 3640–3652, doi:10.1016/j.atmosenv.2006.03.027, 2006.

Kraus, A. and Hofzumahaus, A.: Field measurements of atmospheric photolysis frequencies for  $\text{O}_3$ ,  $\text{NO}_2$ , HCHO,  $\text{CH}_3\text{CHO}$ ,  $\text{H}_2\text{O}_2$ , and HONO by UV spectroradiometry, *J. Atmos. Chem.*, 31, 161–180, doi:10.1023/a:1005888220949, 1998.

Kurtenbach, R., Becker, K. H., Gomes, J. A. G., Kleffmann, J., Lörzer, J. C., Spittler, M., Wiesen, P., Ackermann, R., Geyer, A., and Platt, U.: Investigations of emissions and heterogeneous formation of HONO in a road traffic tunnel, *Atmos. Environ.*, 35, 3385–3394, doi:10.1016/s1352-2310(01)00138-8, 2001.

Lee, B. H., Wood, E. C., Herndon, S. C., Lefer, B. L., Luke, W. T., Brune, W. H., Nelson, D. D., Zahniser, M. S., and Munger, J. W.: Urban measurements of atmospheric nitrous acid: a caveat on the interpretation of the HONO photostationary state, *J. Geophys. Res.-Atmos.*, 118, 12274–12281, doi:10.1002/2013JD020341, 2013.

Lee, J. D., Moller, S. J., Read, K. A., Lewis, A. C., Mendes, L., and Carpenter, L. J.: Year-round measurements of nitrogen oxides and ozone in the tropical North Atlantic marine boundary layer, *J. Geophys. Res.*, 114, D21302, doi:10.1029/2009jd011878, 2009.

**Central London  
HONO budget  
analysis**

J. D. Lee et al.

Title Page

Abstract

Introduction

Conclusions

References

Tables

Figures



Back

Close

Full Screen / Esc

Printer-friendly Version

Interactive Discussion



Legrand, M., Preunkert, S., Frey, M., Bartels-Rausch, Th., Kukui, A., King, M. D., Savarino, J., Kerbrat, M., and Jourdain, B.: Large mixing ratios of atmospheric nitrous acid (HONO) at Concordia (East Antarctic Plateau) in summer: a strong source from surface snow?, *Atmos. Chem. Phys.*, 14, 9963–9976, doi:10.5194/acp-14-9963-2014, 2014.

Levy II, H.: Normal atmosphere: large radical and formaldehyde concentrations predicted, *Science*, 173, 141–143, 1971.

Li, S., Matthews, J., and Sinha, A.: Atmospheric hydroxyl radical production from electronically excited  $\text{NO}_2$  and  $\text{H}_2\text{O}$ , *Science*, 319, 1657–1660, doi:10.1126/science.1151443, 2008.

Li, X., Rohrer, F., Hofzumahaus, A., Brauers, T., Häseler, R., Bohn, B., Broch, S., Fuchs, H., Gomm, S., Holland, F., Jäger, J., Kaiser, J., Keutsch, F. N., Lohse, I., Lu, K., Tillmann, R., Wegener, R., Wolfe, G. M., Mentel, T. F., Kiendler-Scharr, A., and Wahner, A.: Missing gas-phase source of HONO inferred from zeppelin measurements in the troposphere, *Science*, 344, 292–296, doi:10.1126/science.1248999, 2014.

Lidster, R. T., Hamilton, J. F., Lee, J. D., Lewis, A. C., Hopkins, J. R., Punjabi, S., Rickard, A. R., and Young, J. C.: The impact of monoaromatic hydrocarbons on OH reactivity in the coastal UK boundary layer and free troposphere, *Atmos. Chem. Phys.*, 14, 6677–6693, doi:10.5194/acp-14-6677-2014, 2014.

Michoud, V., Kukui, A., Camredon, M., Colomb, A., Borbon, A., Miet, K., Aumont, B., Beekmann, M., Durand-Jolibois, R., Perrier, S., Zapf, P., Siour, G., Ait-Helal, W., Locoge, N., Sauvage, S., Afif, C., Gros, V., Furger, M., Ancellet, G., and Doussin, J. F.: Radical budget analysis in a suburban European site during the MEGAPOLI summer field campaign, *Atmos. Chem. Phys.*, 12, 11951–11974, doi:10.5194/acp-12-11951-2012, 2012.

Michoud, V., Colomb, A., Borbon, A., Miet, K., Beekmann, M., Camredon, M., Aumont, B., Perrier, S., Zapf, P., Siour, G., Ait-Helal, W., Afif, C., Kukui, A., Furger, M., Dupont, J. C., Haeffelin, M., and Doussin, J. F.: Study of the unknown HONO daytime source at a European suburban site during the MEGAPOLI summer and winter field campaigns, *Atmos. Chem. Phys.*, 14, 2805–2822, doi:10.5194/acp-14-2805-2014, 2014.

Monge, M. E., D'Anna, B., Mazri, L., Giroir-Fendler, A., Ammann, M., Donaldson, D. J., and George, C.: Light changes the atmospheric reactivity of soot, *P. Natl. Acad. Sci. USA*, 107, 6605–6609, doi:10.1073/pnas.0908341107, 2010.

Oswald, R., Behrendt, T., Ermel, M., Wu, D., Su, H., Cheng, Y., Breuninger, C., Moravek, A., Mougín, E., Delon, C., Loubet, B., Pommerening-Röser, A., Sörgel, M., Pöschl, U., Hoff-

**Central London  
HONO budget  
analysis**

J. D. Lee et al.

Title Page

Abstract

Introduction

Conclusions

References

Tables

Figures



Back

Close

Full Screen / Esc

Printer-friendly Version

Interactive Discussion



mann, T., Andreae, M. O., Meixner, F. X., and Trebs, I.: HONO emissions from soil bacteria as a major source of atmospheric reactive nitrogen, *Science*, 341, 1233–1235, 2013.

Pollack, I. B., Lerner, B. M., and Ryerson, T. B.: Evaluation of ultraviolet light-emitting diodes for detection of atmospheric NO<sub>2</sub> by photolysis – chemiluminescence, *J. Atmos. Chem.*, 65, 111–125, doi:10.1007/s10874-011-9184-3, 2010.

Qin, M., Xie, P., Su, H., Gu, J., Peng, F., Li, S., Zeng, L., Liu, J., Liu, W., and Zhang, Y.: An observational study of the HONO–NO<sub>2</sub> coupling at an urban site in Guangzhou City, South China, *Atmos. Environ.*, 43, 5731–5742, doi:10.1016/j.atmosenv.2009.08.017, 2009.

Ren, X., Brune, W. H., Oligier, A., Metcalf, A. R., Simpas, J. B., Shirley, T., Schwab, J. J., Bai, C. H., Roychowdhury, U., Li, Y. Q., Cai, C. X., Demerjian, K. L., He, Y., Zhou, X. L., Gao, H. L., and Hou, J.: OH, HO<sub>2</sub>, and OH reactivity during the PMTACS-NY Whiteface Mountain 2002 campaign: observations and model comparison, *J. Geophys. Res.*, 111, D10S03, doi:10.1029/2005JD006126, 2006.

Ren, X., Sanders, J. E., Rajendran, A., Weber, R. J., Goldstein, A. H., Pusede, S. E., Browne, E. C., Min, K.-E., and Cohen, R. C.: A relaxed eddy accumulation system for measuring vertical fluxes of nitrous acid, *Atmos. Meas. Tech.*, 4, 2093–2103, doi:10.5194/amt-4-2093-2011, 2011.

Ren, X. R., Harder, H., Martinez, M., Leshner, R. L., Oligier, A., Simpas, J. B., Brune, W. H., Schwab, J. J., Demerjian, K. L., He, Y., Zhou, X., and Gao, H.: OH and HO<sub>2</sub> chemistry in the urban atmosphere of New York City, *Atmos. Environ.*, 37, 3639–3651, 2003.

Salmon, R. A., Bauguitte, S. J.-B., Bloss, W., Hutterli, M. A., Jones, A. E., Read, K., and Wolff, E. W.: Measurement and interpretation of gas phase formaldehyde concentrations obtained during the CHABLIS campaign in coastal Antarctica, *Atmos. Chem. Phys.*, 8, 4085–4093, doi:10.5194/acp-8-4085-2008, 2008.

Sander, S. P. and Peterson, M. E.: Kinetics of the Reaction HO<sub>2</sub> + NO<sub>2</sub> + M = HO<sub>2</sub>NO<sub>2</sub> + M, *J. Phys. Chem.*, 88, 1566–1571, doi:10.1021/j150652a025, 1984.

Steinbacher, M., Zellweger, C., Schwarzenbach, B., Bugmann, S., Buchmann, B., Ordóñez, C., Prevot, A. S. H., and Hueglin, C.: Nitrogen oxide measurements at rural sites in Switzerland: bias of conventional measurement techniques, *J. Geophys. Res.*, 112, D11307, doi:10.1029/2006jd007971, 2007.

Stemmler, K., Ammann, M., Donders, C., Kleffmann, J., and George, C.: Photosensitized reduction of nitrogen dioxide on humic acid as a source of nitrous acid, *Nature*, 440, 195–198, doi:10.1038/nature04603, 2006.

**Central London  
HONO budget  
analysis**

J. D. Lee et al.

Title Page

Abstract

Introduction

Conclusions

References

Tables

Figures



Back

Close

Full Screen / Esc

Printer-friendly Version

Interactive Discussion



- Stemmler, K., Ndour, M., Elshorbany, Y., Kleffmann, J., D'Anna, B., George, C., Bohn, B., and Ammann, M.: Light induced conversion of nitrogen dioxide into nitrous acid on submicron humic acid aerosol, *Atmos. Chem. Phys.*, 7, 4237–4248, doi:10.5194/acp-7-4237-2007, 2007.
- Stone, D., Evans, M. J., Walker, H., Ingham, T., Vaughan, S., Ouyang, B., Kennedy, O. J., McLeod, M. W., Jones, R. L., Hopkins, J., Punjabi, S., Lidster, R., Hamilton, J. F., Lee, J. D., Lewis, A. C., Carpenter, L. J., Forster, G., Oram, D. E., Reeves, C. E., Bauguutte, S., Morgan, W., Coe, H., Aruffo, E., Dari-Salisburgo, C., Giammaria, F., Di Carlo, P., and Heard, D. E.: Radical chemistry at night: comparisons between observed and modelled HO<sub>x</sub>, NO<sub>3</sub> and N<sub>2</sub>O<sub>5</sub> during the RONOCO project, *Atmos. Chem. Phys.*, 14, 1299–1321, doi:10.5194/acp-14-1299-2014, 2014.
- Stutz, J., Alicke, B., and Neftel, A.: Nitrous acid formation in the urban atmosphere: gradient measurements of NO<sub>2</sub> and HONO over grass in Milan, Italy, *J. Geophys. Res.*, 107, 8192, doi:10.1029/2001jd000390, 2002.
- Su, H., Cheng, Y. F., Cheng, P., Zhang, Y. H., Dong, S., Zeng, L. M., Wang, X., Slanina, J., Shao, M., and Wiedensohler, A.: Observation of nighttime nitrous acid (HONO) formation at a non-urban site during PRIDE-PRD2004 in China, *Atmos. Environ.*, 42, 6219–6232, doi:10.1016/j.atmosenv.2008.04.006, 2008a.
- Su, H., Cheng, Y. F., Shao, M., Gao, D. F., Yu, Z. Y., Zeng, L. M., Slanina, J., Zhang, Y. H., and Wiedensohler, A.: Nitrous acid (HONO) and its daytime sources at a rural site during the 2004 PRIDE-PRD experiment in China, *J. Geophys. Res.-Atmos.*, 113, D14312, doi:10.1029/2007jd009060, 2008b.
- Su, H., Cheng, Y., Oswald, R., Behrendt, T., Trebs, I., Meixner, F. X., Andreae, M. O., Cheng, P., Zhang, Y., and Pöschl, U.: Soil nitrite as a source of atmospheric HONO and OH radicals, *Science*, 333, 1616–1618, doi:10.1126/science.1207687, 2011.
- Trebs, I., Lara, L. L., Zeri, L. M. M., Gatti, L. V., Artaxo, P., Dlugi, R., Slanina, J., Andreae, M. O., and Meixner, F. X.: Dry and wet deposition of inorganic nitrogen compounds to a tropical pasture site (Rondônia, Brazil), *Atmos. Chem. Phys.*, 6, 447–469, doi:10.5194/acp-6-447-2006, 2006.
- Tyndall, G. S., Orlando, J. J., and Calvert, J. G.: Upper Limit for the Rate Coefficient for the Reaction HO<sub>2</sub> + NO<sub>2</sub> → HONO + O<sub>2</sub>, *Environ. Sci. Technol.*, 29, 202–206, doi:10.1021/es00001a026, 1995.
- VandenBoer, T. C., Brown, S. S., Murphy, J. G., Keene, W. C., Young, C. J., Pszenny, A. A. P., Kim, S., Warneke, C., de Gouw, J. A., Maben, J. R., Wagner, N. L., Riedel, T. P., Thorn-

**Central London  
HONO budget  
analysis**

J. D. Lee et al.

Title Page

Abstract

Introduction

Conclusions

References

Tables

Figures



Back

Close

Full Screen / Esc

Printer-friendly Version

Interactive Discussion



ton, J. A., Wolfe, D. E., Dubé, W. P., Öztürk, F., Brock, C. A., Grossberg, N., Lefer, B., Lerner, B., Middlebrook, A. M., and Roberts, J. M.: Understanding the role of the ground surface in HONO vertical structure: high resolution vertical profiles during NACHTT-11, *J. Geophys. Res.*, 118, 10,155–10,171, doi:10.1002/jgrd.50721, 2013.

5 Villena, G., Kleffmann, J., Kurtenbach, R., Wiesen, P., Lissi, E., Rubio, M. A., Croxatto, G., and Rappenglück, B.: Vertical gradients of HONO, NO<sub>x</sub> and O<sub>3</sub> in Santiago de Chile, *Atmos. Environ.*, 45, 3867–3873, doi:10.1016/j.atmosenv.2011.01.073, 2011.

Villena, G., Bejan, I., Kurtenbach, R., Wiesen, P., and Kleffmann, J.: Interferences of commercial NO<sub>2</sub> instruments in the urban atmosphere and in a smog chamber, *Atmos. Meas. Tech.*, 5, 149–159, doi:10.5194/amt-5-149-2012, 2012.

10 Whalley, L. K., Blitz, M. A., Desservettaz, M., Seakins, P. W., and Heard, D. E.: Reporting the sensitivity of laser-induced fluorescence instruments used for HO<sub>2</sub> detection to an interference from RO<sub>2</sub> radicals and introducing a novel approach that enables HO<sub>2</sub> and certain RO<sub>2</sub> types to be selectively measured, *Atmos. Meas. Tech.*, 6, 3425–3440, doi:10.5194/amt-6-3425-2013, 2013.

15 Whalley, L. K., Stone, D., George, I. J., Mertes, S., van Pinxteren, D., Tilgner, A., Herrmann, H., Evans, M. J., and Heard, D. E.: The influence of clouds on radical concentrations: observations and modelling studies of HO<sub>x</sub> during the Hill Cap Cloud Thuringia (HCCT) campaign in 2010, *Atmos. Chem. Phys.*, 15, 3289–3301, doi:10.5194/acp-15-3289-2015, 2015.

20 Wong, K. W., Oh, H.-J., Lefer, B. L., Rappenglück, B., and Stutz, J.: Vertical profiles of nitrous acid in the nocturnal urban atmosphere of Houston, TX, *Atmos. Chem. Phys.*, 11, 3595–3609, doi:10.5194/acp-11-3595-2011, 2011.

Wong, K. W., Tsai, C., Lefer, B., Haman, C., Grossberg, N., Brune, W. H., Ren, X., Luke, W., and Stutz, J.: Daytime HONO vertical gradients during SHARP 2009 in Houston, TX, *Atmos. Chem. Phys.*, 12, 635–652, doi:10.5194/acp-12-635-2012, 2012.

25 Young, D. E., Allan, J. D., Williams, P. I., Green, D. C., Harrison, R. M., Yin, J., Flynn, M. J., Gallagher, M. W., and Coe, H.: Investigating a two-component model of solid fuel organic aerosol in London: processes, PM<sub>1</sub> contributions, and seasonality, *Atmos. Chem. Phys.*, 15, 2429–2443, doi:10.5194/acp-15-2429-2015, 2015.

30 Zhang, N., Zhou, X., Bertman, S., Tang, D., Alaghmand, M., Shepson, P. B., and Carroll, M. A.: Measurements of ambient HONO concentrations and vertical HONO flux above a northern Michigan forest canopy, *Atmos. Chem. Phys.*, 12, 8285–8296, doi:10.5194/acp-12-8285-2012, 2012.

Zhou, X., Civerolo, K., Dai, H., Huang, G., Schwab, J., and Demerjian, K.: Summertime nitrous acid chemistry in the atmospheric boundary layer at a rural site in New York State, *J. Geophys. Res.*, 107, 4590, doi:10.1029/2001jd001539, 2002.

Zhou, X., Gao, H., He, Y., Huang, G., Bertman, S. B., Civerolo, K., and Schwab, J.: Nitric acid photolysis on surfaces in low-NO<sub>x</sub> environments: significant atmospheric implications, *Geophys. Res. Lett.*, 30, 2217, doi:10.1029/2003gl018620, 2003.

Zhou, X., Zhang, N., TerAvest, M., Tang, D., Hou, J., Bertman, S., Alaghmand, M., Shepson, P. B., Carroll, M. A., Griffith, S., Dusanter, S., and Stevens, P. S.: Nitric acid photolysis on forest canopy surface as a source for tropospheric nitrous acid, *Nat. Geosci.*, 4, 440–443, doi:10.1038/NGEO1164, 2011.

ACPD

15, 22097–22139, 2015

**Central London  
HONO budget  
analysis**

J. D. Lee et al.

Title Page

Abstract

Introduction

Conclusions

References

Tables

Figures



Back

Close

Full Screen / Esc

Printer-friendly Version

Interactive Discussion





Central London  
HONO budget  
analysis

J. D. Lee et al.

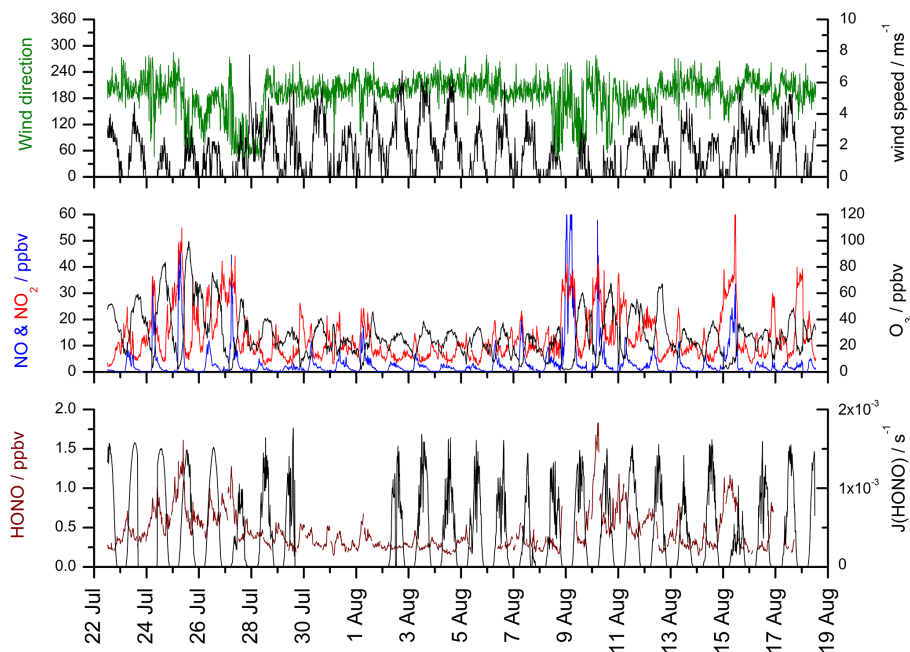


**Figure 1.** Time series of selected data from the ClearLo intensive operation period (July and August 2012). The top panel shows wind speed (black) and wind direction (green); the middle panel shows NO (blue), NO<sub>2</sub> (red) and O<sub>3</sub> (black); and the bottom panel shows HONO (dark red) and  $j(\text{HONO})$  (black). All data is 15 min averaged and plotted as UTC (LT -1 h).

[Title Page](#)[Abstract](#)[Introduction](#)[Conclusions](#)[References](#)[Tables](#)[Figures](#)[Back](#)[Close](#)[Full Screen / Esc](#)[Printer-friendly Version](#)[Interactive Discussion](#)



## Central London HONO budget analysis

J. D. Lee et al.

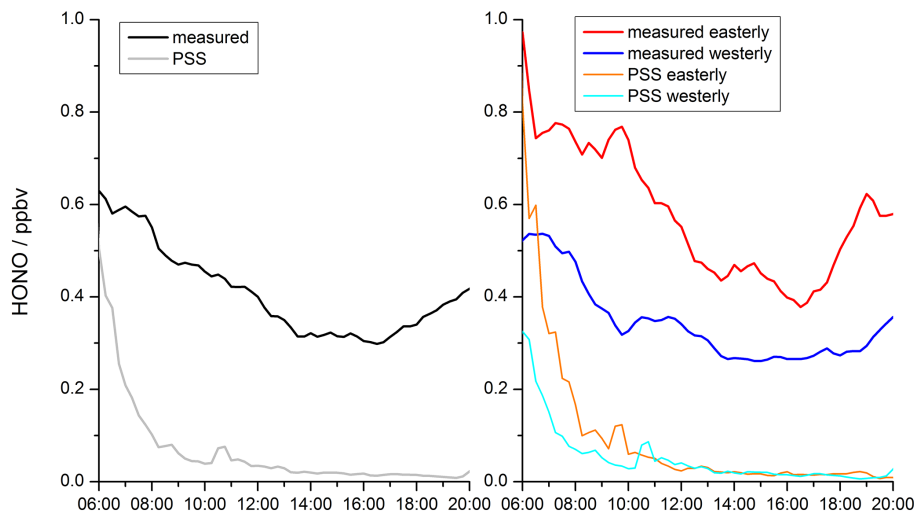


**Figure 3.** Average diurnal profiles (daylight hours) of measured (black) and photostationary state (PSS) calculated (grey) HONO (left panel). The right panel shows averaged diurnal profiles of measured and PSS HONO divided into easterly (red/orange) and westerly (blue/cyan) conditions.

[Title Page](#)[Abstract](#)[Introduction](#)[Conclusions](#)[References](#)[Tables](#)[Figures](#)[◀](#)[▶](#)[◀](#)[▶](#)[Back](#)[Close](#)[Full Screen / Esc](#)[Printer-friendly Version](#)[Interactive Discussion](#)



## Central London HONO budget analysis

J. D. Lee et al.

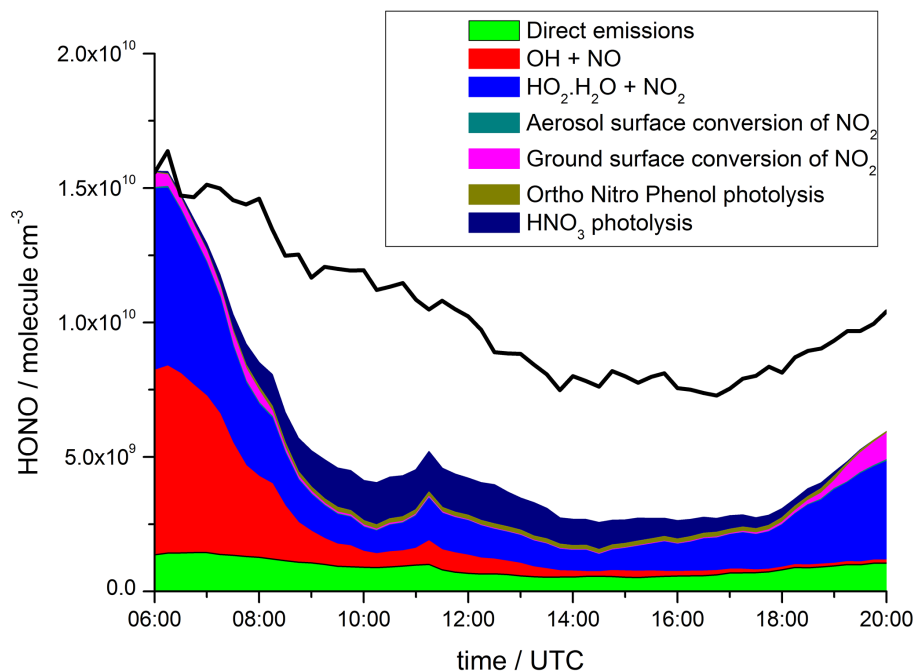


**Figure 5.** Average daytime dirunal profile of the modelled HONO from different sources shown as a compound area plot. Also plotted (black trace) is the measured HONO.

[Title Page](#)[Abstract](#)[Introduction](#)[Conclusions](#)[References](#)[Tables](#)[Figures](#)[◀](#)[▶](#)[◀](#)[▶](#)[Back](#)[Close](#)[Full Screen / Esc](#)[Printer-friendly Version](#)[Interactive Discussion](#)



## Central London HONO budget analysis

J. D. Lee et al.

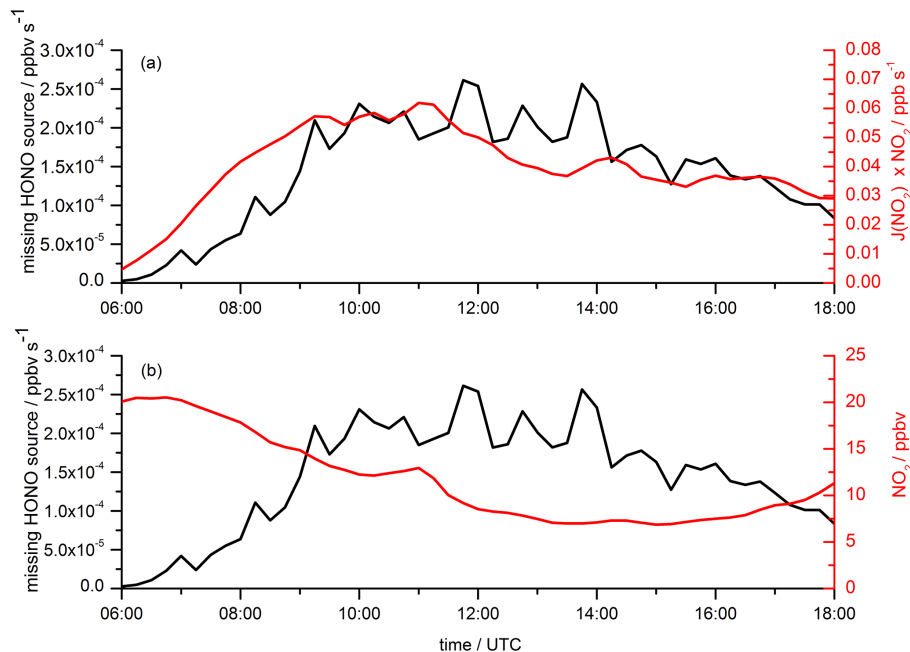


**Figure 7.** Average diurnal profiles of the missing HONO source (black traces) plotted with (as red traces) **(a)**  $\text{NO}_2 \times j(\text{NO}_2)$  and **(b)**  $\text{NO}_2$ .

Title Page

Abstract

Introduction

Conclusions

References

Tables

Figures



Back

Close

Full Screen / Esc

Printer-friendly Version

Interactive Discussion



## Central London HONO budget analysis

J. D. Lee et al.

Title Page

Abstract

Introduction

Conclusions

References

Tables

Figures



Back

Close

Full Screen / Esc

Printer-friendly Version

Interactive Discussion

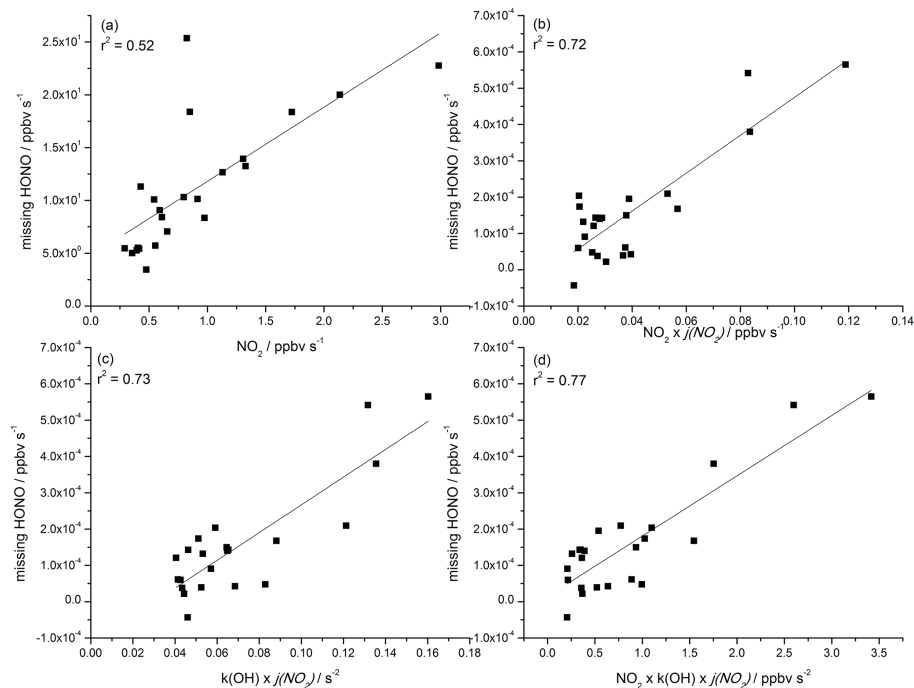


**Figure 8.** Daytime averaged (07:00–19:00) missing HONO source plotted against **(a)** NO<sub>2</sub>, **(b)** NO<sub>2</sub> × j(NO<sub>2</sub>), **(c)** k(OH) × j(NO<sub>2</sub>), **(d)** NO<sub>2</sub> × k(OH) × j(NO<sub>2</sub>).

Central London  
HONO budget  
analysis

J. D. Lee et al.

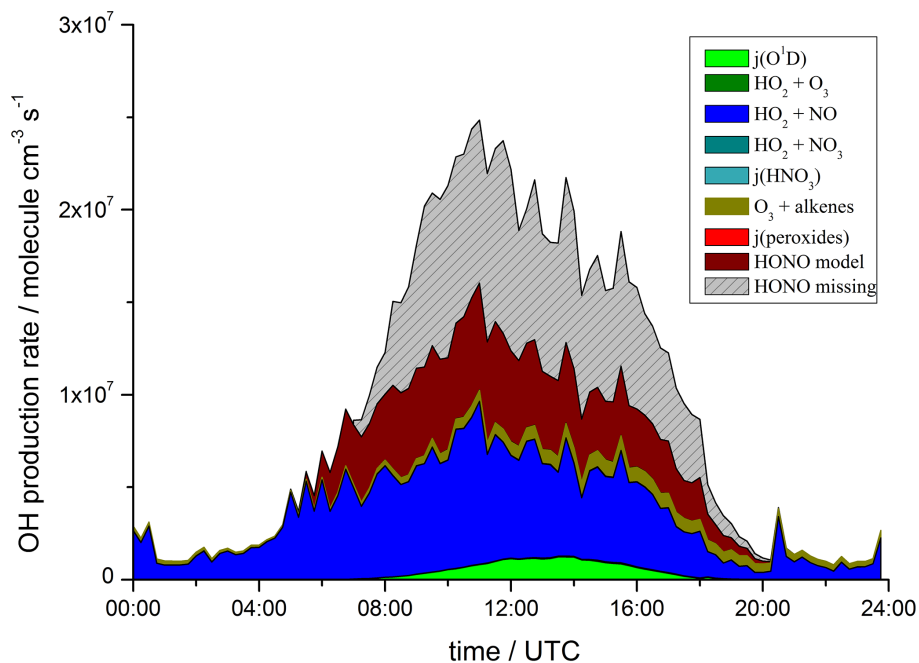


**Figure 9.** Average diurnal profile of gross OH production rates from different initiation and propagation sources calculated by the model.

[Title Page](#)[Abstract](#)[Introduction](#)[Conclusions](#)[References](#)[Tables](#)[Figures](#)[◀](#)[▶](#)[◀](#)[▶](#)[Back](#)[Close](#)[Full Screen / Esc](#)[Printer-friendly Version](#)[Interactive Discussion](#)

## Central London HONO budget analysis

J. D. Lee et al.

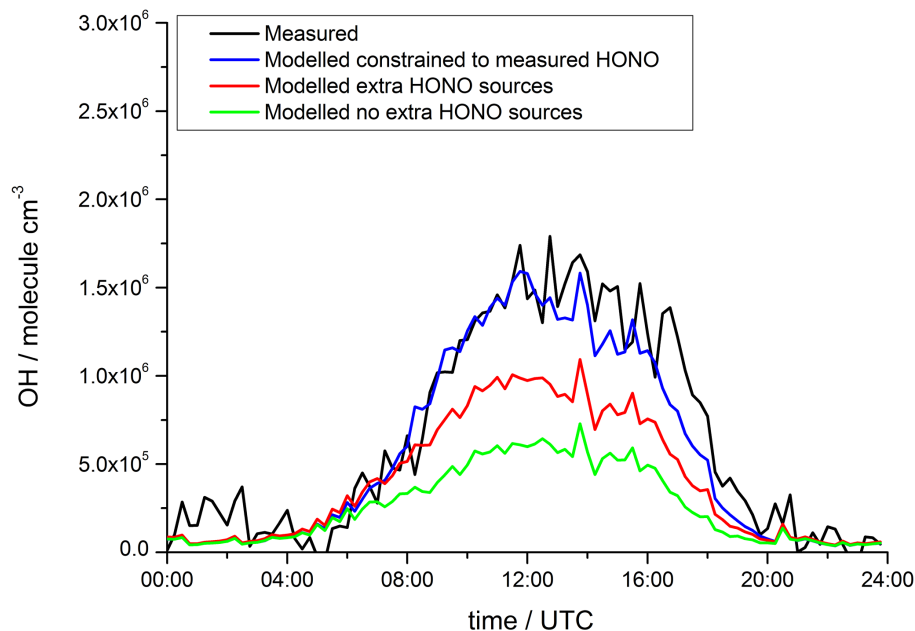


**Figure 10.** Average diurnal profile of OH, showing measured (black), modelled unconstrained to HONO with only NO + OH as a HONO sources (green), modelled unconstrained to HONO including additional HONO sources (red – see text for details) and model constrained to measured HONO (blue).

[Title Page](#)[Abstract](#)[Introduction](#)[Conclusions](#)[References](#)[Tables](#)[Figures](#)[◀](#)[▶](#)[◀](#)[▶](#)[Back](#)[Close](#)[Full Screen / Esc](#)[Printer-friendly Version](#)[Interactive Discussion](#)